Micro-Roughness Effects in (Elasto)Hydrodynamic Lubrication Including a Mass-Flow Preserving Cavitation Model

Guy Bayada, Sébastien Martin, Carlos Vazquez

Micro-Roughness Effects in (Elasto)Hydrodynamic Lubrication Including a Mass-Flow Preserving Cavitation Model

Guy Bayada

INSA de Lyon / LAMCOS CNRS-UMR 5514 / ICJ CNRS-UMR 5208
Bât. Léonard de Vinci, 21 av. Jean Capelle
69621 Villeurbanne cedex, France

Sébastien Martin

INSA de Lyon / ICJ CNRS-UMR 5208
Bât. Léonard de Vinci, 21 av. Jean Capelle
69621 Villeurbanne cedex, France

Carlos Vázquez

Universidade da Coruña
Facultade de Informática / Dept. de Matemáticas
Campus Elviña, 15071-A Coruña, España

Abstract

An average Reynolds equation is proposed for predicting the effects of deterministic periodic roughness, taking JFO mass flow preserving cavitation model and elasto-hydrodynamic effects into account. For this, the asymptotic model is based upon double scale analysis approach. The average Reynolds equation can be used both for microscopic interasperity cavitation and macroscopic one. The validity of such a model is verified by numerical experiments.

Key words: Elastohydrodynamic; Lubrication; Roughness.

Email addresses: guy.bayada@insa-lyon.fr (Guy Bayada), sebastien.martin@insa-lyon.fr (Sébastien Martin), carlosv@udc.es (Carlos Vázquez).

Preprint *1 September 2005*

NOMENCLATURE

h_r	=	rigid gap
$h_{[p]}$	=	effective gap (including deformation)
h_0	=	minimum thickness of the rigid gap
R	=	sphere or cylinder section radius
k	=	Hertz kernel
p	=	pressure
p_0, $p_1 \ldots$	=	approximations of the pressure
θ	=	saturation
θ_0	=	microscopic homogenized saturation
Θ_i, Θ	=	macro-homogenized saturations
$x = (x_1, x_2)$	=	space variables
$y = (y_1, y_2)$	=	microscale variables
$Y =]0,1[\times]0,1[$	=	rescaled microcell
$(A^\star_{[p]})_{ij}$, $A^{(i,\star)}_{[p]}$	=	homogenized coefficients
$B^{(i,\star)}_{[p]}$, $B^{(i,0)}_{[p]}$	=	homogenized coefficients
$w^{(i)}_{[p_0]}$, $\chi^{(i,0)}_{[p_0]}$	=	auxiliary functions defined on Y
α	=	piezoviscosity coefficient
$\partial/\partial n$	=	normal derivative
ε	=	roughness spacing
$\overline{\cdot}^Y$	=	average operator with respect to y
L	=	length of the journal bearing
R_b	=	bearing radius
R_j	=	journal radius
R_m	=	mean radius
Γ_a, Γ_0, $\Gamma_\sharp$, $\Gamma_\star$	=	boundaries of the device
c	=	clearance
ρ	=	eccentricity of the bearing
p_a	=	supply pressure
μ	=	viscosity
v_0	=	velocity of the bearing
a_r	=	amplitude of the roughness
W	=	load
θ_{in}	=	supply flow

1 Introduction

In this paper, it is explained how the double scale procedure, already used to obtain average equations with periodic roughness in the case of rigid bearings [1–3], can be extended to EHD problems including cavitation and starvation. The JFO mass flow preserving model is used, including pressure and saturation as unknown functions. This model takes into account both microcavitation (due to the microroughness) and macrocavitation (due to the diverging part of the gap). Average equation can be easily solved for some specific roughness patterns (transverse, longitudinal) exactly in the same way as the initial EHD problem with cavitation. Numerical results are given for both purely hydrodynamic and EHD point-contact problems, for a two dimensional device.

2 Basic equations

Our studied cavitation model, like the Elrod algorithm and its variants [4,5], views the film as a mixture. It does not, however, make the assumption of liquid compressibility in the full film area as in [6] and some other papers. The flow obeys the following "universal" Reynolds equation (here written in a dimensionless form) through all the gap in which the pressure cavitation is assumed to be zero in the cavitation area. Moreover, the lubricant is piezo-viscous so that the viscosity obeys the Barus law (notice that other laws may be taken into account). The effective gap contains a rigid contribution and an elastic one, which is given by the Hertz law (for local contacts):

$$\sum_{i=1}^{2} \frac{\partial}{\partial x_i} \left(h_{[p]}^3 \; e^{-\alpha p} \; \frac{\partial p}{\partial x_i} \right) = \frac{\partial \; \theta h_{[p]}}{\partial x_1}, \tag{1}$$

$$p \geq 0, \tag{2}$$

$$0 \leq \theta \leq 1, \tag{3}$$

$$p \; (1 - \theta) = 0, \tag{4}$$

p is the pressure (assumed to be a positive function), θ is the relative mixture density, $h_{[p]}$ the real film thickness, x_1 is the direction of the effective relative shear velocity of the device, while x_2 is the transverse direction. Here, $h_{[p]}$, which is the effective gap between two close surfaces, contains a given rigid contribution h_r and an elastic one, which strongly depends on the main unknown p (lubricant pressure) in the following nonlocal form:

$$h_{[p]}(x) = h_r(x) + \int_{\Omega} k(x, z) p(z) \; dz,$$

the kernel k depending on the kind of contact. The classical approximation of the rigid gap [7] is given by the expression

$$h_r(x) = \begin{cases} h_0 + \dfrac{x_1^2 + x_2^2}{2R}, & \text{for ball bearings,} \\ h_0 + \dfrac{x_1^2}{R}, & \text{for linear bearings,} \end{cases} \tag{5}$$

that represents a parabolic approximation for a given sphere-plane (point contact) or cylinder-plane (line contact) gap, R being the sphere or cylinder section radius. The positive constant h_0 corresponds to the gap at the point nearest to contact. Now, let us introduce the general property of the kernel k:

$$k(x,z) = \begin{cases} c_0 \ \log\Big|\dfrac{c_1 - z_1}{x_1 - z_1}\Big|, & \text{for line contacts,} \\ \dfrac{c_0}{\sqrt{(x_1 - z_1)^2 + (x_2 - z_2)^2}}, & \text{for point contacts,} \end{cases} \tag{6}$$

where $c_0 > 0$ and $c_1 \geq \max\{\Big|x_1\Big|, \ x \in \overline{\Omega}\}$.

3 Asymptotic expansion

Let us suppose that the roughness is periodically reproduced in the two x_1 and x_2 directions from an elementary cell Y (or "miniature bearing" in Tonder's terminology). We denote by ε the ratio of the homothetic transformation passing from the elementary cell $Y = Y_1 \times Y_2$ to the real bearing and by $y_1 = x_1/\varepsilon$ and $y_2 = x_2/\varepsilon$ the local variables (see FIG. 1).

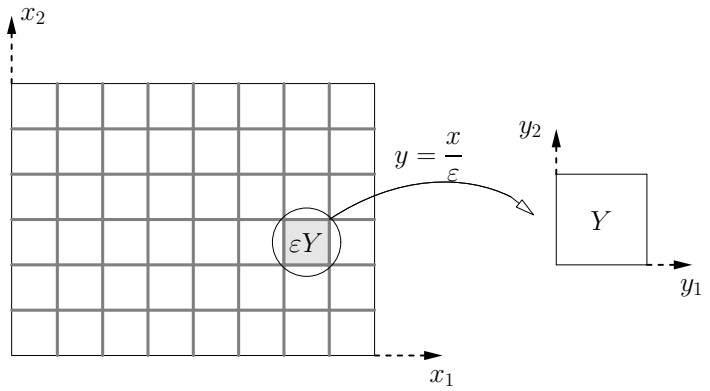

Fig. 1. Macroscopic domain and elementary cells

Let us now consider gaps that can be written as $h_r(x, x/\varepsilon)$. Introducing now the fast variables y_1 and y_2, it appears that the new expression for the gap

is $h_r(x,y)$ in the two-scale approach. The combined computation in terms of (x_1,x_2) or (y_1,y_2) is an important feature of the method. It is convenient to consider first x and y as independent variables and to replace next y by x/ε (see [1]).
In this section, we recall the main tools that allow the derivation of average equations. The process has the same feature as the one corresponding to the hydrodynamic case, which can be found in [3]. The equations should be read as

$$\sum_{j=1}^{2} \frac{\partial}{\partial x_j} \left\{ \left(h_{[p]} \left(x, \frac{x}{\varepsilon} \right) \right)^3 e^{-\alpha p} \frac{\partial p}{\partial x_j} \right\} = \frac{\partial}{\partial x_1} \left\{ \theta \; h_{[p]} \left(x, \frac{x}{\varepsilon} \right) \right\},$$
$$p \geq 0, \quad 0 \leq \theta \leq 1, \quad p(1-\theta) = 0,$$

with the additional notation:

$$h_{[p]} \left(x, \frac{x}{\varepsilon} \right) = h_r \left(x, \frac{x}{\varepsilon} \right) + \int_{\Omega} k(x,z) \; p(z) \; dz.$$

We shall look for an asymptotic expansion of the solutions:

$$p(x) = p_0(x) + \varepsilon p_1 \left(x, \frac{x}{\varepsilon} \right) + \varepsilon^2 p_2 \left(x, \frac{x}{\varepsilon} \right) + ..., \tag{7}$$

$$\theta(x) = \theta_0 \left(x, \frac{x}{\varepsilon} \right), \tag{8}$$

p_0 being a positive function, and each unknown p_i $(i \geq 1)$ and θ_0 being function of (x,y). The problem of the boundary conditions to be satisfied by the p_i is somewhat difficult but may be summarized so:

(i) The natural boundary conditions on (p,θ) are assigned to p_0 and an equivalent saturation linked to θ_0, which will be developped in next subsection.
(ii) The function p_i, $i \geq 1$, are Y periodic, i.e. periodic in the two variables y_1, y_2, for each value of (x_1,x_2).

To be noticed that, unlike of p, we do not introduce an asymptotic expansion for θ. This can be explained by observing the evolution of p and θ as ε tends to 0. Clearly, the oscillations of the pressure are decreasing and p tends to a smooth function (namely p_0 which, actually, does not depend on the fast variable as it will be pointed out further). This is not the case for θ and an asymptotic smooth limit cannot be considered.
We shall see later that the functions p_i, $i \geq 1$, are defined up to an additive constant. Moreover, from Equations (21)–(23), the following properties hold:

$$p_0(x) \geq 0, \tag{9}$$

$$0 \leq \theta_0(x,y) \leq 1, \tag{10}$$
$$p_0(x,y)\ (1-\theta_0(x,y)) = 0. \tag{11}$$

Putting Equations (7) and (8) into Equation (20), one can write, by an identification procedure, the following macroscopic / microscopic decomposition:

• Macroscopic equation:

$$\sum_{j=1}^{2} \frac{\partial}{\partial x_j} \left\{ \overline{h^3_{[p_0]}(x,y)\ e^{-\alpha p_0(x)}\ \left(\frac{\partial p_0}{\partial x_j}(x) + \frac{\partial p_1}{\partial y_j}(x,y) \right)}^{Y} \right\} = \frac{\partial}{\partial x_1} \left\{ \overline{\theta_0(x,y)\ h_{[p_0]}(x,y)}^{Y} \right\}, \tag{12}$$

where $\overline{u}^Y$ denotes the local average of any Y periodic function u:

$$\overline{u}^Y(x) = \frac{1}{[Y]} \int_Y u(x,y)\ dy.$$

• Microscopic equation: for each x, we have

$$\sum_{j=1}^{2} \frac{\partial}{\partial y_j} \left\{ h^3_{[p_0]}(x,y)\ e^{-\alpha p_0(x)}\ \left(\frac{\partial p_0}{\partial x_j}(x) + \frac{\partial p_1}{\partial y_j}(x,y) \right) \right\} = \frac{\partial}{\partial x_1} \Big\{ \theta_0(x,y)\ h_{[p_0]}(x,y) \Big\}. \tag{13}$$

Notice that, in the earlier equation, the variable x only plays the role of a parameter.
Of course, the macroscopic equation (12) is not sufficient to describe a complete asymptotic model: indeed, we have to eliminate p_1 in order to get a single pressure-saturation equation. For this, we use the microscopic equation (13). Thus we can represent p_1 as a function of p_0 and θ_0 in a more usable form. We define $w^{(i)}_{[p_0]}$, $\chi^{(i),0}_{[p_0]}$ and $\chi^{(i,\star)}_{[p_0]}$ $(i = 1, 2)$ as the Y periodic solutions (up to an additive constant) of the following local problems:

$$\sum_{j=1}^{2} \frac{\partial}{\partial y_j} \left(h^3_{[p_0]}\ e^{-\alpha p_0}\ \frac{\partial w^{(i)}_{[p_0]}}{\partial y_j} \right) = \frac{\partial h^3_{[p_0]}}{\partial y_i}, \tag{14}$$

$$\sum_{j=1}^{2} \frac{\partial}{\partial y_j} \left(h^3_{[p_0]}\ e^{-\alpha p_0}\ \frac{\partial \chi^{(i,0)}_{[p_0]}}{\partial y_j} \right) = \frac{\partial \theta_0 h_{[p_0]}}{\partial y_i}, \tag{15}$$

$$\sum_{j=1}^{2} \frac{\partial}{\partial y_j} \left(h_{[p_0]}^3 \; e^{-\alpha p_0} \; \frac{\partial \chi_{[p_0]}^{(i,\star)}}{\partial y_j} \right) = \frac{\partial h_{[p_0]}}{\partial y_i}. \tag{16}$$

Notice that, contrary to the local problems in the purely hydrodynamic case which have been studied in [3], the local problems in the EHL problem highly depend on the macroscopic pressure p_0, which is due to the piezoviscosity and elastic deformation only.
The solution of Equation (13) reduces to:

$$\begin{aligned} p_1(x,y) = e^{\alpha p_0(x)} \; \chi_{[p_0]}^{(1,0)}(x,y) - \frac{\partial p_0}{\partial x_1}(x) \; w_{[p_0]}^{(1)}(x,y) \\ - \frac{\partial p_0}{\partial x_2}(x) \; w_{[p_0]}^{(2)}(x,y). \end{aligned} \tag{17}$$

By exchanging the integral and the derivation symbols, and after some calculations, Equation (12) becomes:

$$\sum_{i,j} \frac{\partial}{\partial x_i} \left\{ \left(A_{[p_0]}^{\star} \right)_{ij} e^{-\alpha p_0} \; \frac{\partial p_0}{\partial x_j} \right\} = \sum_i \frac{\partial}{\partial x_i} \left\{ B_{[p_0]}^{(i,0)} \right\},$$

where ($i, j = 1, 2$ and $j \neq i$)

$$\begin{aligned} \left(A_{[p_0]}^{\star} \right)_{ii} &= \overline{h_{[p_0]}^3 - h_{[p_0]}^3 \frac{\partial w_{[p_0]}^{(i)}}{\partial y_i}}^{Y}, \\ \left(A_{[p_0]}^{\star} \right)_{ij} &= \overline{-h_{[p_0]}^3 \frac{\partial w_{[p_0]}^{(j)}}{\partial y_i}}^{Y} = \overline{-h_{[p_0]}^3 \frac{\partial w_{[p_0]}^{(i)}}{\partial y_j}}^{Y} = \left(A_{[p_0]}^{\star} \right)_{ji}, \end{aligned}$$

and also

$$B_{[p_0]}^{(1,0)} = \overline{\theta_0 h_{[p_0]} - h_{[p_0]}^3 \frac{\partial \chi_{[p_0]}^{(1,0)}}{\partial y_1}}^{Y}, \quad B_{[p_0]}^{(2,0)} = \overline{-h_{[p_0]}^3 \frac{\partial \chi_{[p_0]}^{(1,0)}}{\partial y_2}}^{Y}.$$

In the end, we can also define the normalized coefficients

$$\begin{aligned} B_{[p_0]}^{(1,\star)} &= \overline{h_{[p_0]} - h_{[p_0]}^3 \frac{\partial \chi_{[p_0]}^{(1,\star)}}{\partial y_1}}^{Y}, \quad B_{[p_0]}^{(2,\star)} = \overline{-h_{[p_0]}^3 \frac{\partial \chi_{[p_0]}^{(1,\star)}}{\partial y_2}}^{Y}, \\ \Theta_1 &= \frac{B_{[p_0]}^{(1,0)}}{B_{[p_0]}^{(1,\star)}}, \qquad \Theta_2 = \frac{B_{[p_0]}^{(2,0)}}{B_{[p_0]}^{(2,\star)}}, \end{aligned}$$

which provide the following generalized Reynolds equation:

$$\sum_{i,j=1}^{2} \frac{\partial}{\partial x_i} \left\{ \left(A^{\star}_{[p_0]} \right)_{ij} e^{-\alpha p_0} \frac{\partial p_0}{\partial x_j} \right\} = \sum_{i=1}^{2} \frac{\partial}{\partial x_i} \left\{ \Theta_i B^{(i,\star)}_{[p_0]} \right\}. \tag{18}$$

Moreover it is obvious that the following properties hold:

$$p_0 \geq 0, \quad p_0(1-\Theta_i) = 0, \quad (i=1,2). \tag{19}$$

Equations (18) and (19) deal with any periodic roughness pattern. To be noticed is the fact that the differential operator is no more of the Reynolds type since extra terms $\partial^2 p_0/\partial x_i \partial x_j$ appear. The right-hand side also contains an additive term in the x_2 direction. However, the link between p_0 and Θ_i is not so clear. This is a major obstacle which prevents to get a tractable equation. In fact, the pressure / double saturation problem lacks some properties: we cannot prove that the so-called anisotropic saturations Θ_i are functions with values in $[0,1]$. However, it is possible to define in a rigorous way (see [2]) a solution with an isotropic saturation $\Theta = \Theta_1 = \Theta_2$ and $0 \leq \Theta \leq 1$. Moreover, under some additional assumptions (see [3]), we can prove some complementary results. Thus, when dealing with transverse roughness and longitudinal roughness, the homogenized coefficients can be easily simplified and given in an explicit form. In both cases, the asymptotic system has the same structure than the initial (roughless) one, i.e.

$$\sum_{i=1}^{2} \frac{\partial}{\partial x_i} \left\{ A^{(i,\star)}_{[p_0]} \; e^{-\alpha p_0} \frac{\partial p_0}{\partial x_i} \right\} = \frac{\partial \Theta B^{(1,\star)}_{[p_0]}}{\partial x_1}, \tag{20}$$

$$p_0 \geq 0, \tag{21}$$

$$0 \leq \Theta \leq 1, \tag{22}$$

$$p_0 \; (1-\Theta) = 0. \tag{23}$$

▷ *Transverse roughness*: the homogenized coefficients are

$$A^{(1,\star)}_{[p_0]} = \frac{1}{\overline{h^{-3}_{[p_0]}}^{Y}}, \quad A^{(2,\star)}_{[p_0]} = \overline{h^{3}_{[p_0]}}^{Y}, \quad B^{(1,\star)}_{[p_0]} = \frac{\overline{h^{-2}_{[p_0]}}^{Y}}{\overline{h^{-3}_{[p_0]}}^{Y}},$$

the link between the macroscopic saturation Θ and the microscopic one θ_0 being given by:

$$\Theta(x) = \left(\frac{1}{\overline{h^{-2}_{[p_0]}}^{Y}} \; \overline{\left(\frac{\theta_0}{h^{2}_{[p_0]}} \right)}^{Y} \right)(x).$$

▷ *Longitudinal roughness*: the homogenized coefficients are

$$A^{(1,\star)}_{[p_0]} = \overline{h^3_{[p_0]}}^Y, \quad A^{(2,\star)}_{[p_0]} = \frac{1}{\overline{h^{-3}_{[p_0]}}^Y}, \quad B^{(1,\star)}_{[p_0]} = \overline{h_{[p_0]}}^Y,$$

the link between the macroscopic saturation Θ and the microscopic one θ_0 being given by:

$$\Theta(x) = \left(\frac{\overline{\theta_0 h_{[p_0]}}^Y}{\overline{h_{[p_0]}}^Y} \right)(x).$$

All the earlier results are valid for both elastohydrodynamic and hydrodynamic cases and, thus, generalize the ones that have been stated in [3]. As an important feature, Θ is not the average of the microscopic saturation θ_0 but contains some anisotropic effects due to the roughness direction. In the purely hydrodynamic case, one can prove some additional results, corresponding to a wide class of two dimensional roughness patterns. Indeed, suppose that h_r can be written under the form

$$h_r(x,y) = h_1(x,y_1)\, h_2(x,y_2),$$

then we get the following (hydrodynamic) homogenized equation

$$\begin{aligned} &\sum_{i=1}^{2} \frac{\partial}{\partial x_i} \left\{ A^{(i,\star)} \frac{\partial p_0}{\partial x_i} \right\} = \frac{\partial}{\partial x_1} \left\{ \Theta B^{(1,\star)} \right\}, \\ &p_0 \geq 0, \quad 0 \leq \Theta \leq 1, \quad p_0(1-\Theta) = 0, \end{aligned}$$

with

$$A^{(i,\star)} = \frac{\overline{h_j^3}^Y}{\overline{h_i^{-3}}^Y}, \quad B^{(1,\star)} = \frac{\overline{h_1^{-2}}^Y}{\overline{h_1^{-3}}^Y}\, \overline{h_2}^Y,$$

the link between the macroscopic and the microscopic saturations being given by

$$\Theta = \frac{1}{\overline{h_2}^Y\, \overline{h_1^{-2}}^Y} \overline{\left(\frac{\theta_0 h_2}{h_1^2} \right)}^Y.$$

4 Numerical results

In this section, the numerical simulation of a micro(elasto)hydrodynamic contact is performed to illustrate the theoretical results of convergence stated in the previous sections. For the numerical solution of the ε dependent problems and their corresponding homogenized one, we propose the characteristics method adapted to steady state problems to deal with the the convection term combined with a finite element spatial discretization. These numerical techniques has been already successfully used in previous papers dealing with hydrodynamic aspects (see [8,9]), and elastohydrodynamic aspects (see, for instance, [10,11]).

In TABLE 1, we present the functional coefficients $A^{(1,\star)}_{[p_0]}$, $A^{(2,\star)}_{[p_0]}$, $B^{(1,\star)}_{[p_0]}$ that appear in the homogenized problem for purely transverse and purely longitudinal roughness cases which have been partially computed with MATHEMATICA Software Package. Suppose that the domain to be considered is a rectangular one

$$(a,b)\times(c,d),$$

and that the rough (elasto)hydrodynamic gap can be written under the form

$$h_{[p]}\left(x,\frac{x}{\varepsilon}\right)=h_r(x)+h_d[p](x)+\begin{cases}\alpha_1\sin\left(\dfrac{2\pi}{\varepsilon}\dfrac{x_1-a}{b-a}\right), & \text{(transverse roughness)}\\ \alpha_2\sin\left(\dfrac{2\pi}{\varepsilon}\dfrac{x_2-c}{d-c}\right), & \text{(longitudinal roughness)}\end{cases}$$

where h_r (resp. $h_d[p]$) denotes the roughless rigid (resp. elastic) contribution to the gap and the remaining term describes the roughness patterns in the purely transverse or longitudinal case.

	Transverse roughness	Longitudinal roughness
$h_{[p]}(x,y)$	$h_r(x)+h_d[p](x)+\alpha_1\sin(2\pi y_1)$	$h_r(x)+h_d[p](x)+\alpha_2\sin(2\pi y_2)$
$A^{(1,\star)}_{[p_0]}$	$2\dfrac{\left((h_r+h_d[p])^2-\alpha_1^2\right)^{5/2}}{2(h_r+h_d[p])^2+h_r^2}$	$(h_r+h_d[p])^3+\dfrac{3}{2}\,(h_r+h_d[p])\,\alpha_2^2$
$A^{(2,\star)}_{[p_0]}$	$(h_r+h_d[p])^3+\dfrac{3}{2}\,(h_r+h_d[p])\,\alpha_1^2$	$2\,\dfrac{\left((h_r+h_d[p])^2-\alpha_2^2\right)^{5/2}}{2(h_r+h_d[p])^2+\alpha_2^2}$
$B^{(1,\star)}_{[p_0]}$	$2(h_r+h_d[p])\,\dfrac{(h_r+h_d[p])^2-\alpha_1^2}{2(h_r+h_d[p])^2+\alpha_1^2}$	$h_r+h_d[p]$

Table 1
Elastohydrodynamic homogenized coefficients

4.1 Hydrodynamic case

We adress the numerical simulation of journal bearing devices with circumferential supply of lubricant. The mechanical characteristics of the device are given by:

- length: $L = 0.019\ m$,
- bearing radius: $R_b = 0.0164975\ m$,
- journal radius: $R_j = 0.01647\ m$,
- mean radius: $R_m = 0.5\ (R_b + R_j)$,
- clearance : $c = R_b - R_j$,
- eccentricity: $\rho = 0.2$.

The physical characteristics of the regime are the following one:

- supply pressure: $p_a = 283000\ Pa$,
- lubricant viscosity: $\mu = 0.02\ Pa.s$,
- shear velocity: $v_0 = 17.247\ m/s$.

The earlier problem leads to the following set of equations

$$\sum_{i=1}^{2} \frac{\partial}{\partial x_i}\left(h^3\ \frac{\partial p}{\partial x_i}\right) = \Lambda \frac{\partial\ \theta h}{\partial x_1},$$
$$p \geq 0, \quad 0 \leq \theta \leq 1, \quad p\ (1-\theta) = 0,$$

with $\Lambda = 6\mu v_0$, and the real roughless gap shoud be read as

$$h(x) = c\,(1 + \rho\ \cos(x_1/R_m))\,.$$

The equations have to be solved on the domain $(0, 2\pi R_m) \times (0, L/2)$ (see the developped configuration on FIG.2) with the following boundary conditions:

- $p = p_a$ on Γ_a, $p = 0$ on Γ_0,
- periodic conditions on $\Gamma_\sharp$, i.e. p and $6\mu v_0\ \theta h - h^3 \dfrac{\partial p}{\partial x_1}$ are $2\pi R_m x_1$ periodic.

To be noticed is the fact that the corresponding homogenized boundary conditions can be written as follows (using the terminology of TABLE 1):

- $p_0 = p_a$ on Γ_a, $p_0 = 0$ on Γ_0,
- periodic conditions on $\Gamma_\sharp$, i.e. p_0 and $6\mu v_0\ \Theta B^{(1,\star)} - A^{(1,\star)} \dfrac{\partial p_0}{\partial x_1}$ are $2\pi R_m x_1$ periodic.

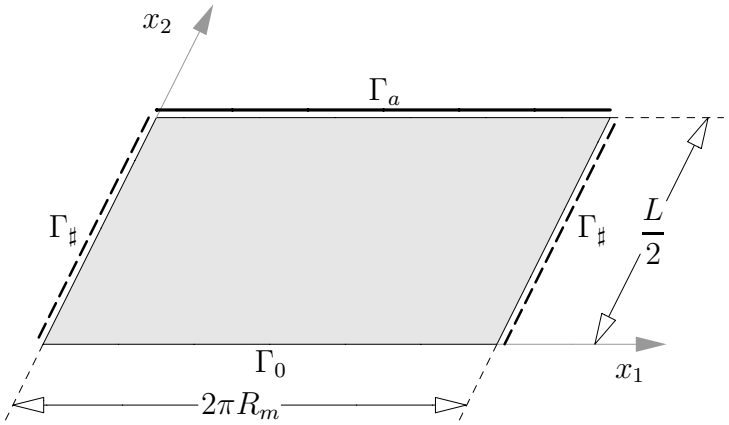

Fig. 2. Journal bearing domain

Actually, we consider transverse roughness patterns and the gap should be read as:

$$h\left(x, \frac{x}{\varepsilon}\right) = c\left(1 + \rho\ \cos\left(x_1/R_m\right) + a_r\ \sin\left(\frac{2\pi}{\varepsilon}\frac{x_1}{R_m}\right)\right)$$

with $a_r/\rho = 0.2$, a_r denoting the amplitude parameter of the roughness.
FIG.3 and 4 (resp. 5 and 6) show the pressure and saturation profiles for $\varepsilon = 1/15$ (resp. $\varepsilon = 1/30$) compared to the homogenized solution, at a fixed $x_2^0 = L/4$. Thus, it allows to observe the roughness effects in the x_1 direction. The amplitude of the pressure oscillations tend to be damped, although the amplitude of the saturation oscillations stay the same in cavitated areas. As it was noticed in [3], it points out the fact that when the number of roughness patterns increases, the pressure behaves as a smooth function, namely $p_0(x)$, while the saturation behaves as a highly oscillating function, namely $\theta_0(x, x/\varepsilon)$. Thus, the pressure tends to a smooth one as ε tends to 0, while the saturation is always oscillating. To be noticed on FIG.4 and 6 is the fact that the cavitation area is made of two macrocavitation zones (for $\varepsilon = 1/15$, $x_1 > 0.06$ and $x_1 < 0.01$) and a lot of microcavitation zones.
FIG.7 and 8 represent the homogenized pressure and saturation in the real domain.

4.2 Elastohydrodyamic case

The numerical tests deal with a dimensionless problem, as described in Section 2: the domain is $(-4, 2) \times (2, 2)$. The considered rigid contribution to the gap is a normalized one:

$$h_0 + \frac{x_1^2 + x_2^2}{2}$$

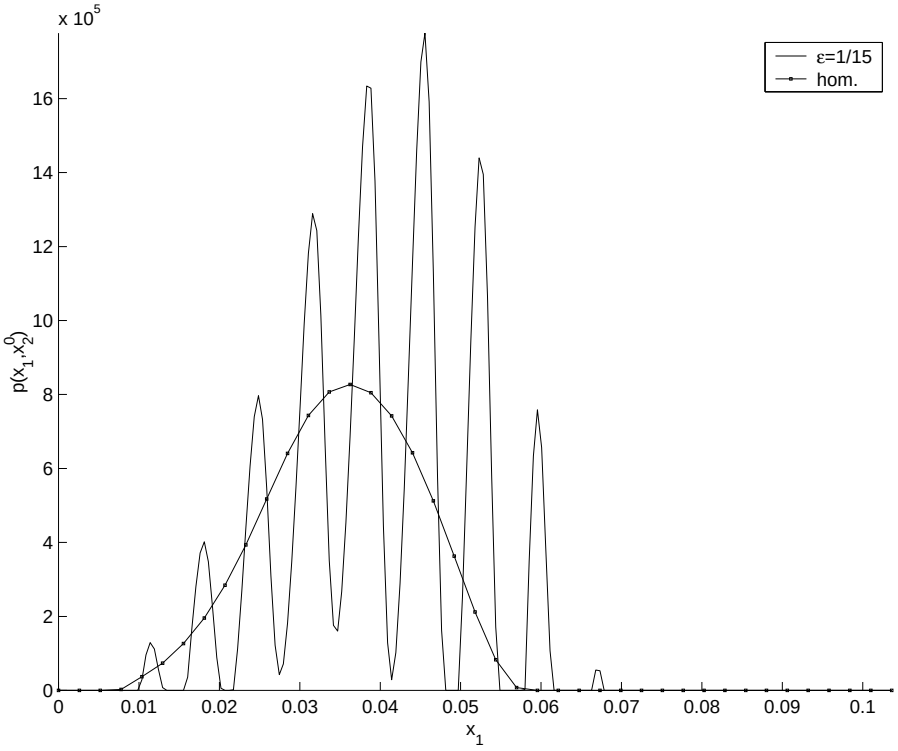

Fig. 3. Hydrodynamic pressure for $\varepsilon = 1/15$ at $x_2^0 = L/4$

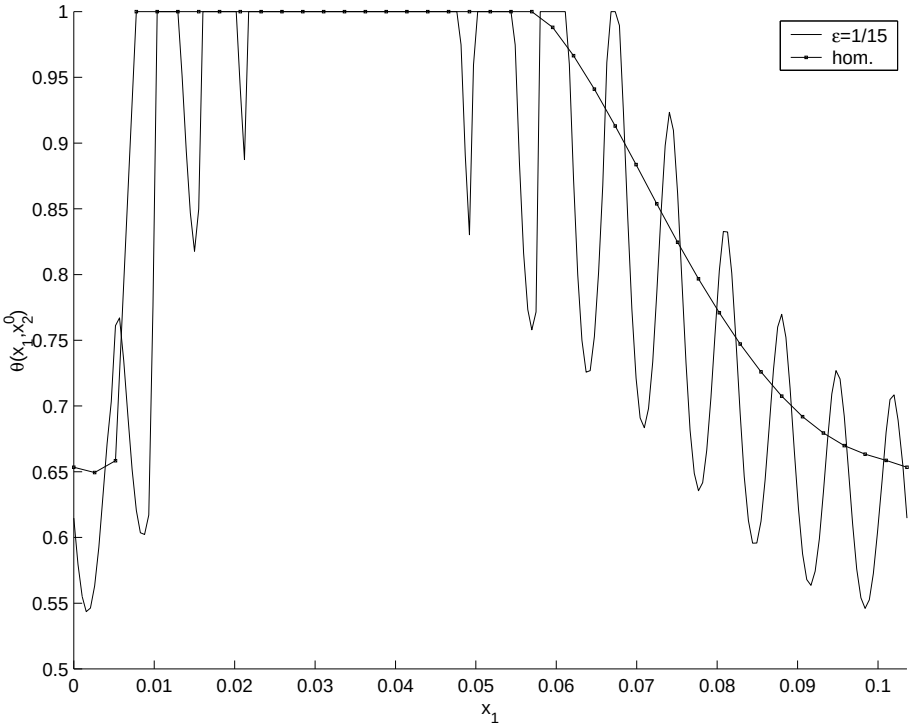

Fig. 4. Hydrodynamic saturation for $\varepsilon = 1/15$ at $x_2^0 = L/4$

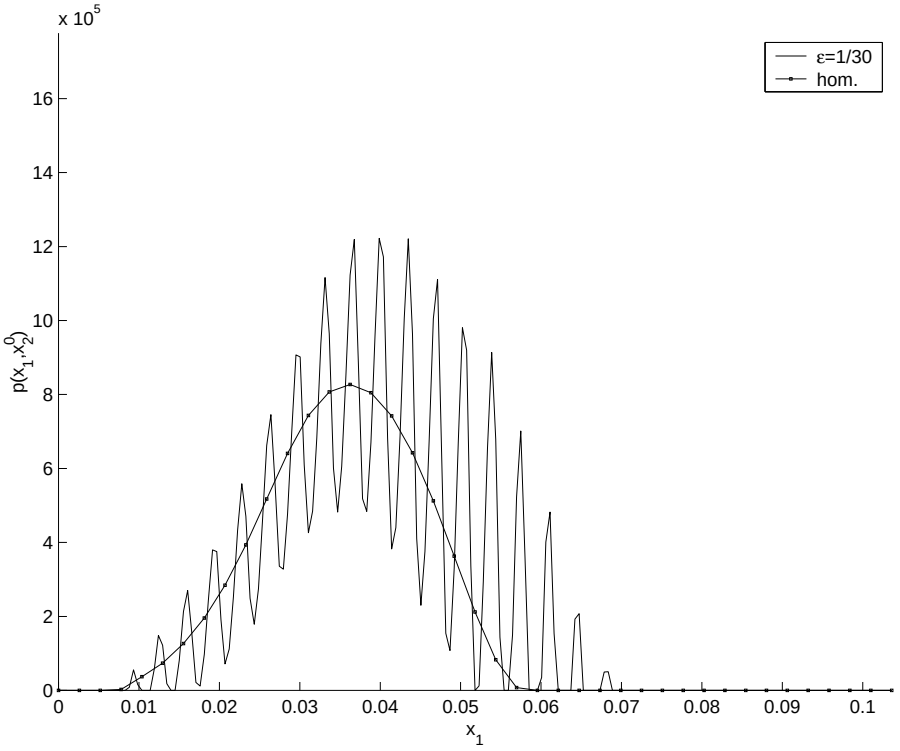

Fig. 5. Hydrodynamic pressure for $\varepsilon = 1/30$ at $x_2^0 = L/4$

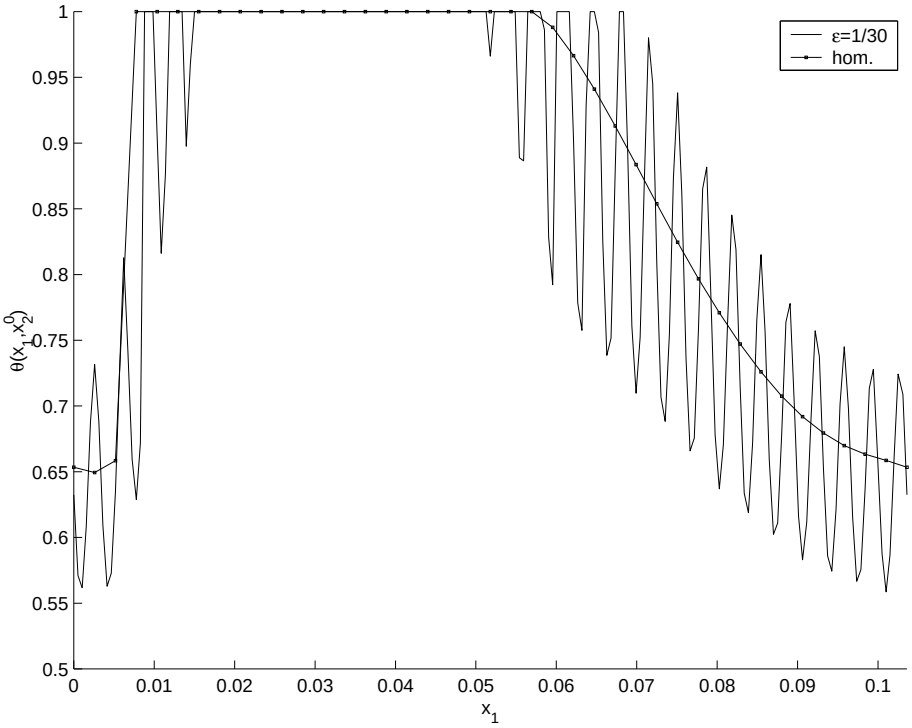

Fig. 6. Hydrodynamic saturation for $\varepsilon = 1/30$ at $x_2^0 = L/4$

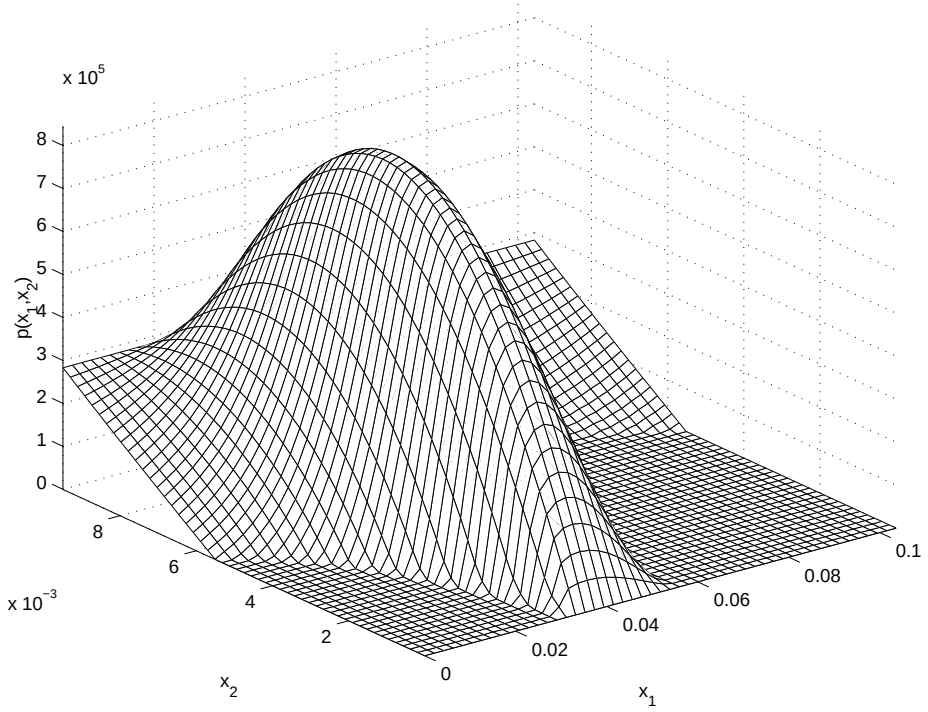

Fig. 7. Homogenized hydrodynamic pressure in the whole device

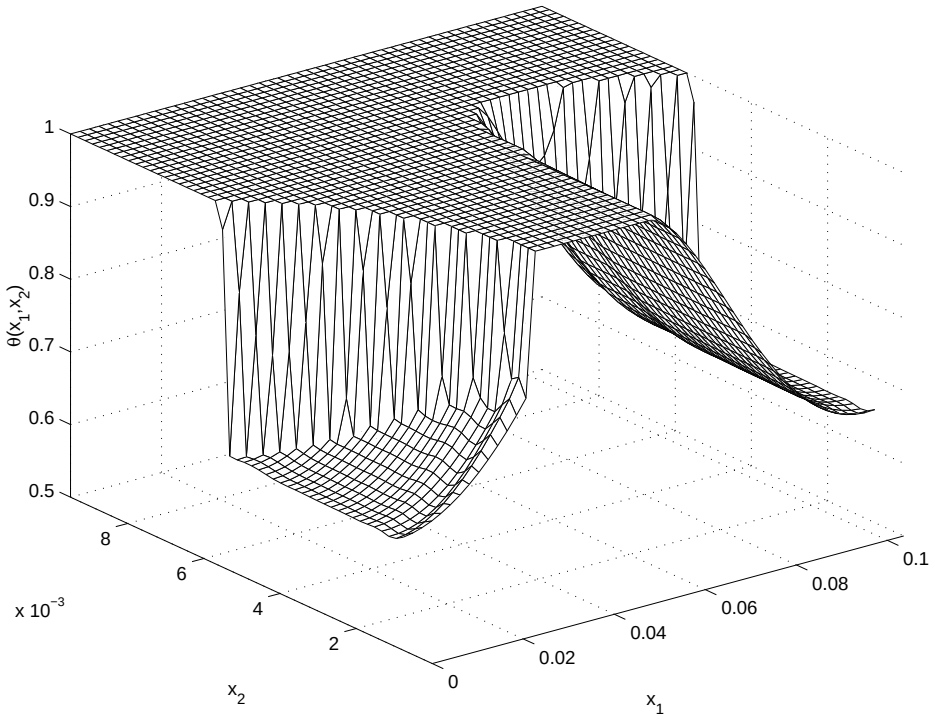

Fig. 8. Homogenized hydrodynamic saturation in the whole device

where h_0 denotes the minimum thickness. Since a point contact has been considered, we choose the following Hertz model:

$$k(x,z) = \frac{2}{\pi^2} \frac{1}{\sqrt{(x_1 - z_1)^2 + (x_2 - z_2)^2}}$$

The equations are:

$$\sum_{i=1}^{2} \frac{\partial}{\partial x_i} \left(h[p]^3 \; e^{-\alpha p} \; \frac{\partial p}{\partial x_i} \right) = \frac{\partial \; \theta h[p]}{\partial x_1},$$
$$p \geq 0, \quad p \; (1-\theta) = 0 \quad 0 \leq \theta \leq 1,$$

The boundary conditions are the following ones:

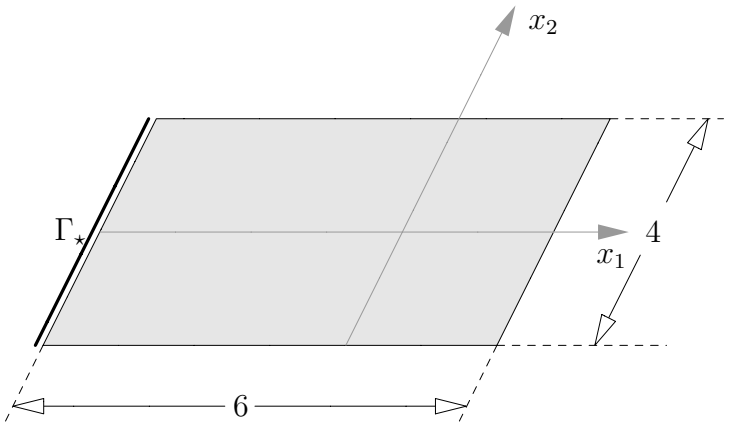

Fig. 9. Normalized EHL domain

- flow condition on $\Gamma_\star$: $\theta h[p] - h[p]^3 \dfrac{\partial p}{\partial x_1} = \theta_{in} h[p]$, with $\theta_{in} = 0.3$,
- $p = 0$ elsewhere.

The corresponding homogenized boundary conditions can be written as:

- flow condition on $\Gamma_\star$: $\Theta B^{(1,\star)}_{[p_0]} - A^{(1,\star)}_{[p_0]} \dfrac{\partial p_0}{\partial x_1} = \theta_{in} C^{(\star)}_{[p_0]}$, with

$$C^{(\star)}_{[p_0]} = \left(h_r + h_d[p] \right)_{|\Gamma_\star} .$$

- $p_0 = 0$ elsewhere.

The chosen values of h_0 and α will be discussed further.

4.2.1 Transverse roughness

Numerical tests have been made for the following rigid contribution to the gap:

$$h_0 + \frac{x_1^2 + x_2^2}{2} + h_0 \ \sin\left(2\pi \frac{x_1 + 4}{6\ \varepsilon}\right)$$

with $h_0 = 0.5$ and different values of ε. Moreover, the piezoviscosity has been taken to $\alpha = 1$. Homogenized coefficients in the transverse roughness cases are deduced from TABLE 1 (see page 10).
FIG.10, 12 and 14 represent the pressure, saturation and deformation profiles at $x_2^0 = 0$ in the roughless case ($\varepsilon = +\infty$), a deterministic rough case ($\varepsilon = 1/30$) and the homogenized case. To be observed is the fact that the homogenized profiles give a satisfying approach of the roughness effects ($\varepsilon = 1/30$), unlike the roughless profiles: indeed, the pressure profiles given in FIG.10 evidence the fact that the homogenized pressure is a smooth version of the rough pressure. Similarly, by FIG.12, the homogenized saturation can be seen as an average version of the rough saturation, up to anisotropic effects. On FIG.14, we observe that the rough deformation (corresponding to $\varepsilon = 1/30$) nearly coincides with the homogenized one: this is due to the regularizing effects of the Hertz kernel. In fact, the deformation profile has a rate of convergence which is much greater than the pressure profile.
FIG.11, 13 and 15 represent the homogenized pressure, saturation and deformation in the domain.

4.2.2 Longitudinal roughness

Numerical tests have been made for the following rigid contribution to the gap:

$$h_0 + \frac{x_1^2 + x_2^2}{2} + h_0 \ \sin\left(2\pi \frac{x_2 + 2}{4\ \varepsilon}\right)$$

with $h_0 = 0.5$ and different values of ε. Moreover, the piezoviscosity has been taken to $\alpha = 1$. Let us notice that, again, Homogenized coefficients in the transverse roughness cases are deduced from TABLE 1 (see page 10).
FIG.16 and 17 represent the pressure and deformation profiles at $x_1^0 = -0.4$, in the x_2 direction (in order to observe the roughness effects). This choice corresponds to the maximum pressure in the homogenized case, which is attained at $(x_1^0, x_2^0) = (-0.4, 0)$. Of course, the saturation profile is omitted, for all corresponding saturation functions would be identically equal to 1 (no cavitation in this part of the domain). Significantly, the size of the oscillations for the pressure are damped easily, and convergence of the rough solution to the homogenized one is illustrated on both figures. Similarly, pressure / saturation / deformation curves are omitted, for they are similar to the ones observed in the transverse roughness case.

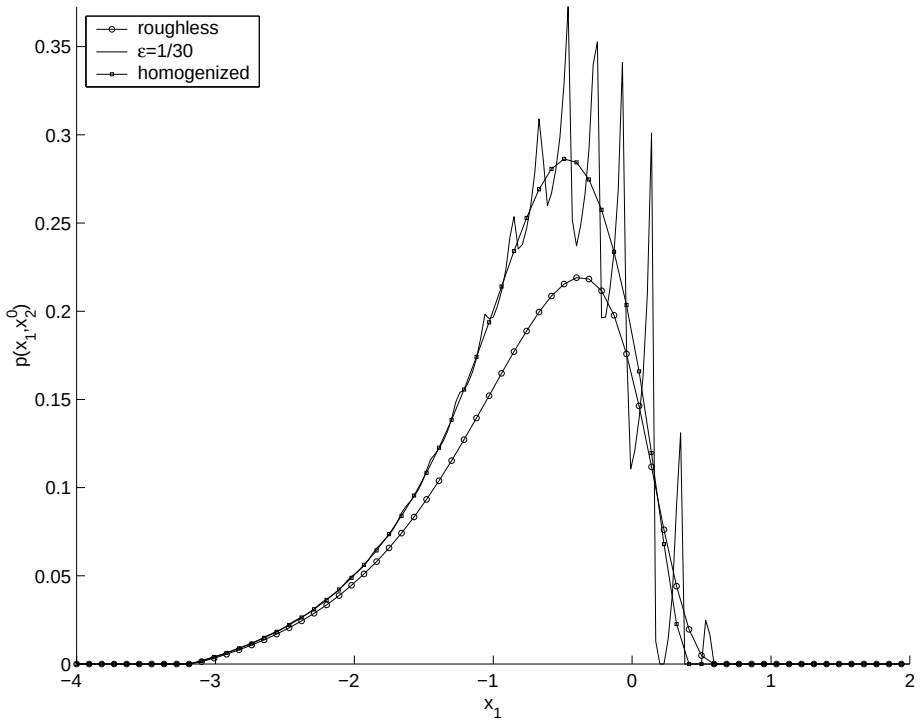

Fig. 10. EHL pressure with transverse roughness patterns at $x_2^0 = 0$

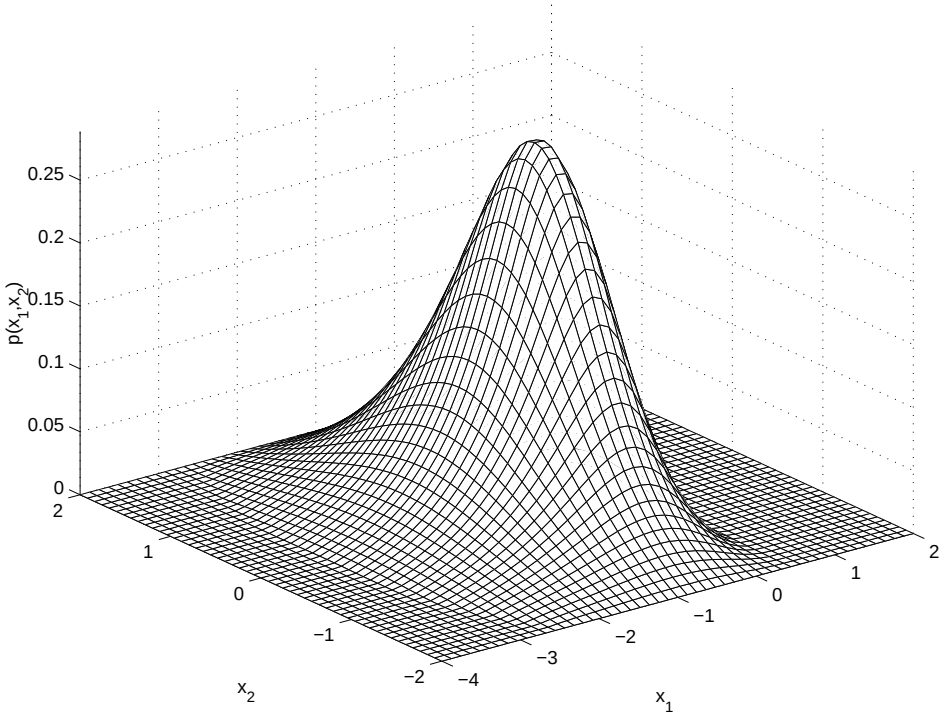

Fig. 11. Homogenized EHL pressure in the whole domain

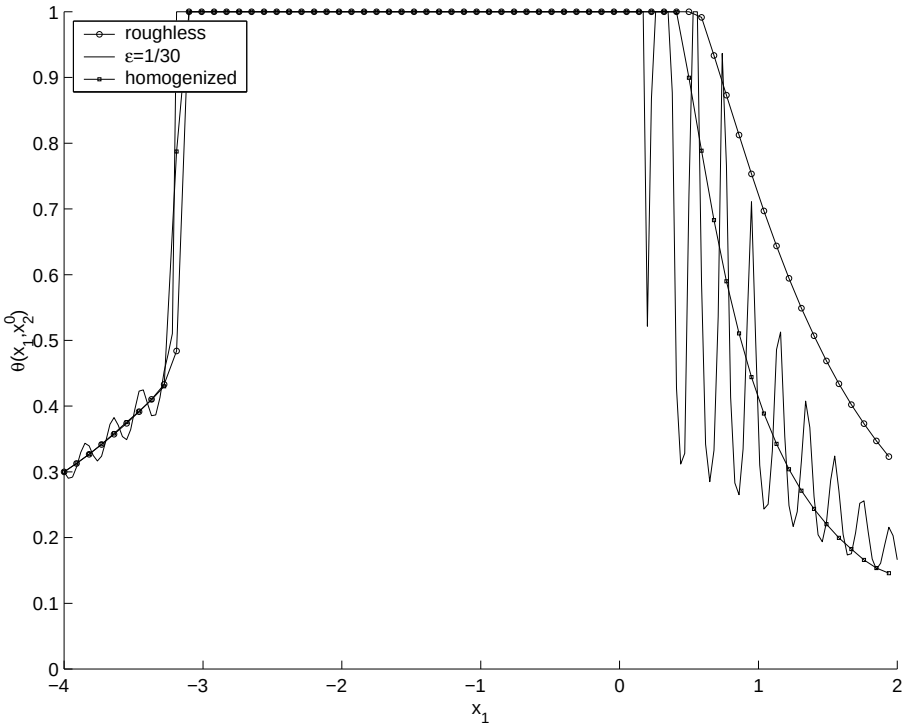

Fig. 12. EHL saturation with transverse roughness patterns at $x_2^0 = 0$

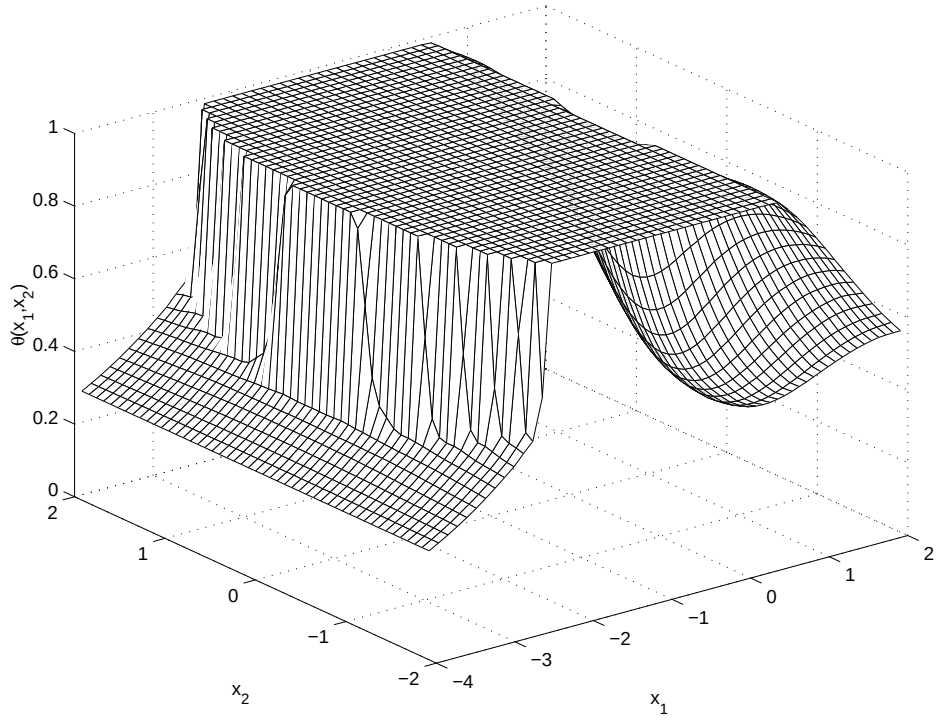

Fig. 13. Homogenized EHL saturation in the whole domain

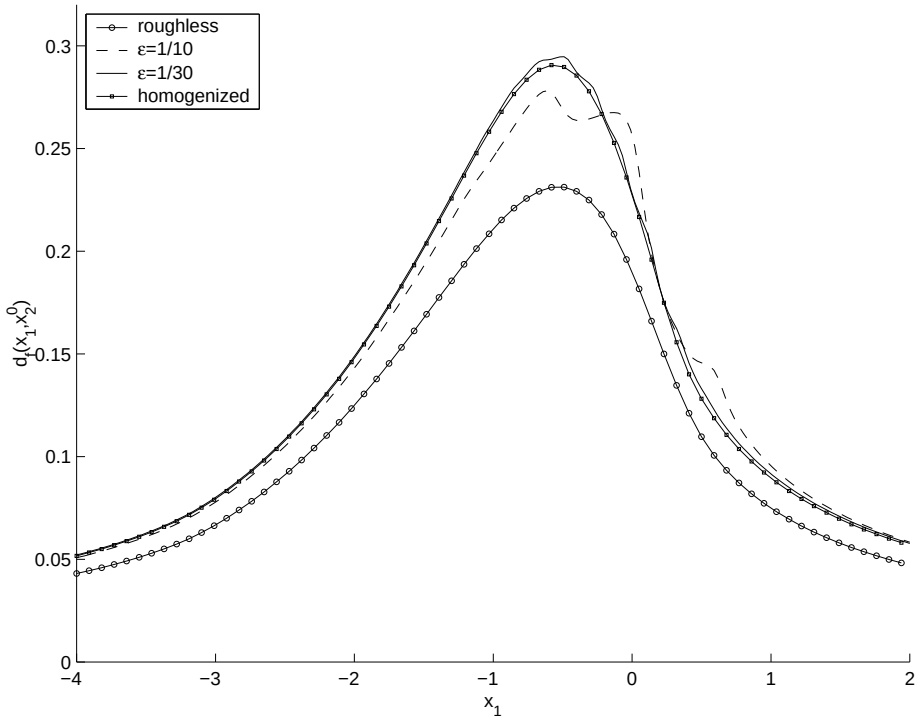

Fig. 14. EHL deformation with transverse roughness patterns at $x_2^0 = 0$

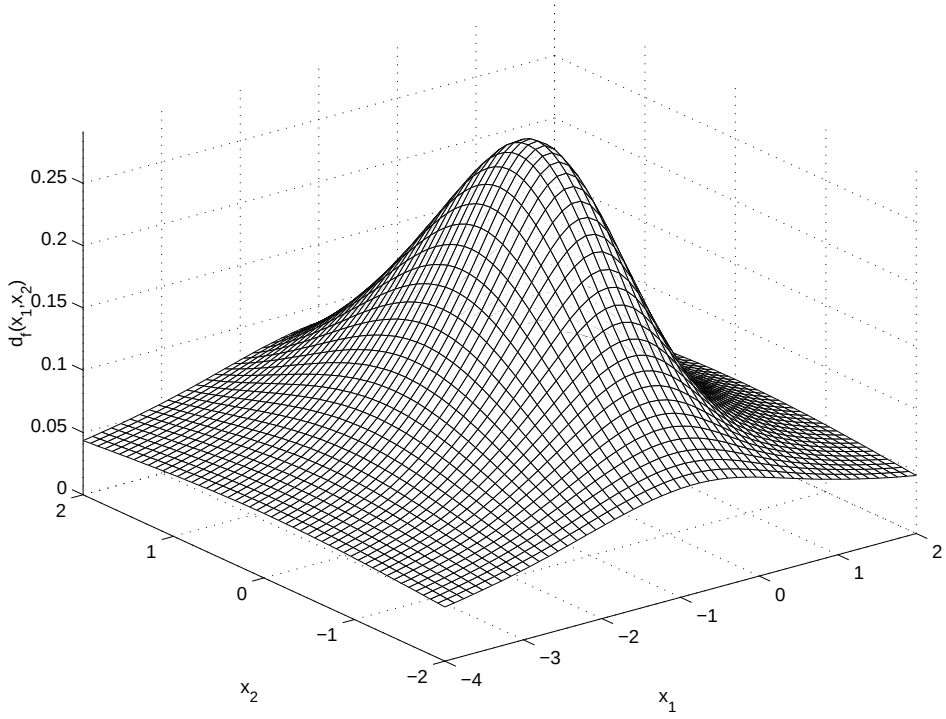

Fig. 15. Homogenized EHL deformation in the whole domain

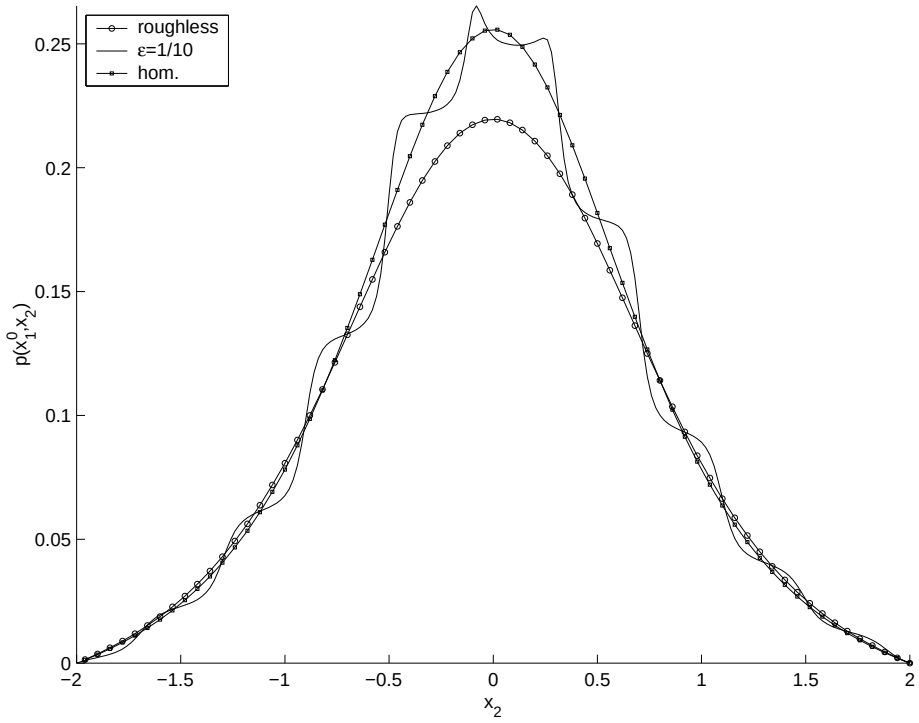

Fig. 16. EHL pressure with longitudinal roughness patterns at $x_1^0 = -0.4$

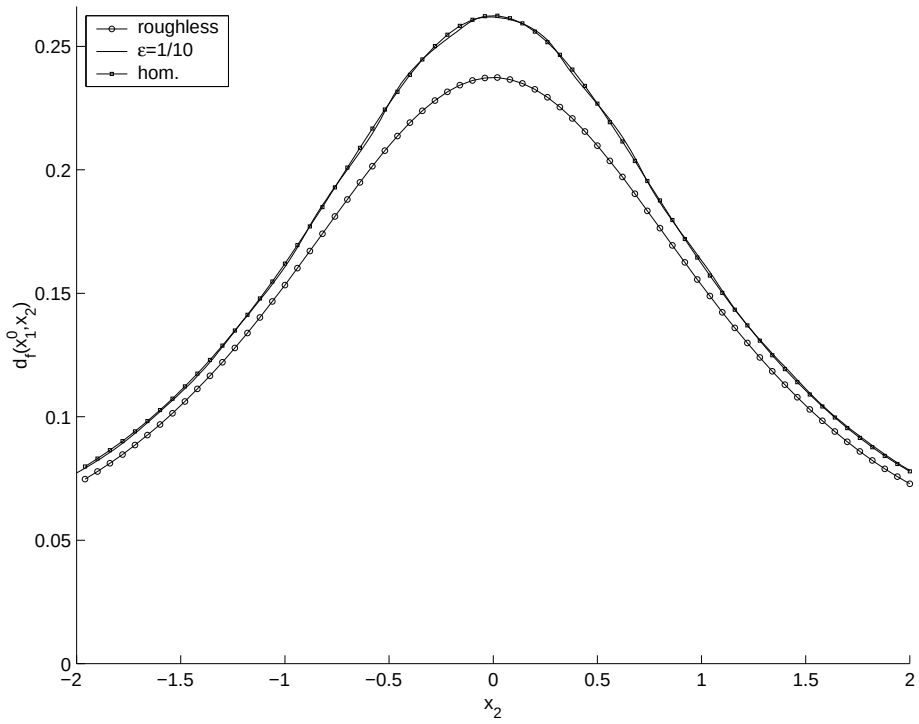

Fig. 17. EHL deformation with longitudinal roughness patterns at $x_1^0 = -0.4$

4.2.3 Influence of the roughness effects in EHL and hydrodynamic cases

FIG.18 and 19 show the difference of roughness effects between a purely hydrodynamic (isoviscous) configuration and an elastohydrodynamic (piezoviscous) configuration. The data are the same as in the transverse roughness case (see Subsection 4.2.1), except for the rough gap whose amplitude of roughness patterns is modified in order to prevent contact between the surfaces in the hydrodynamic case: thus, the gap is

$$h_0 + \frac{x_1^2 + x_2^2}{2} + 0.7\ h_0\ \sin\left(2\pi \frac{x_1 + 4}{6\ \varepsilon}\right),$$

all other numerical data being the same as before (in particular for the value of h_0 and the piezoviscosity parameter α). It can be noticed that the elevation of the pressure due to the roughness patterns is less important in the EHL case than in the purely hydrodynamic case. This is due to the fact that the elastic deformation tends to damp the additional load corresponding to the roughness. It has little influence over the saturation distribution, although the homogenization process does not allow to get microcavitation effects which do exist when a deterministic rough pattern is considered. Though, this analysis also states that microcavitation effects tend to vanish as ε tends to 0.

4.2.4 Influence of the roughness over the load

Numerical tests have been made for the following rigid contribution to the gap:

$$h_0 + \frac{x_1^2 + x_2^2}{2} + a_r\ \sin\left(2\pi \frac{x_1 + 4}{6\ \varepsilon}\right)$$

with $h_0 \in \{0.5, 1, 1.5, 2\}$ and $a_r/h_0 \in \{0.2, 0.4, 0.6, 0.8, 1\}$. Moreover, the elastic contribution to the gap is the one given at the beginning of Subsection 4.2, and piezoviscosity has been taken to $\alpha = 0$ (isoviscous case). Results are given on FIG.20, showing the influence of the minimum thickness $h_r - a_r$ over the load W for different values of h_0. Results are taken from the analysis of the corresponding homogenized solution.

4.2.5 Influence of the piezoviscosity

We focus on the behaviour of the solution with respect to the piezoviscosity parameter α. Numerical data are the same than in the elastohydrodynamic case with transverse roughness (Subsection 4.2.1), except that we take into account piezoviscous properties of the lubricant: $\alpha = 0$, 1, 2 or 3.

FIG.21 and 22 represent the pressure and deformation profiles at $x_2^0 = 0$ in the homogenized case. They illustrate the trend induced by the piezoviscosity parameter: the peak pressure and the peak deformation increase with α. Only

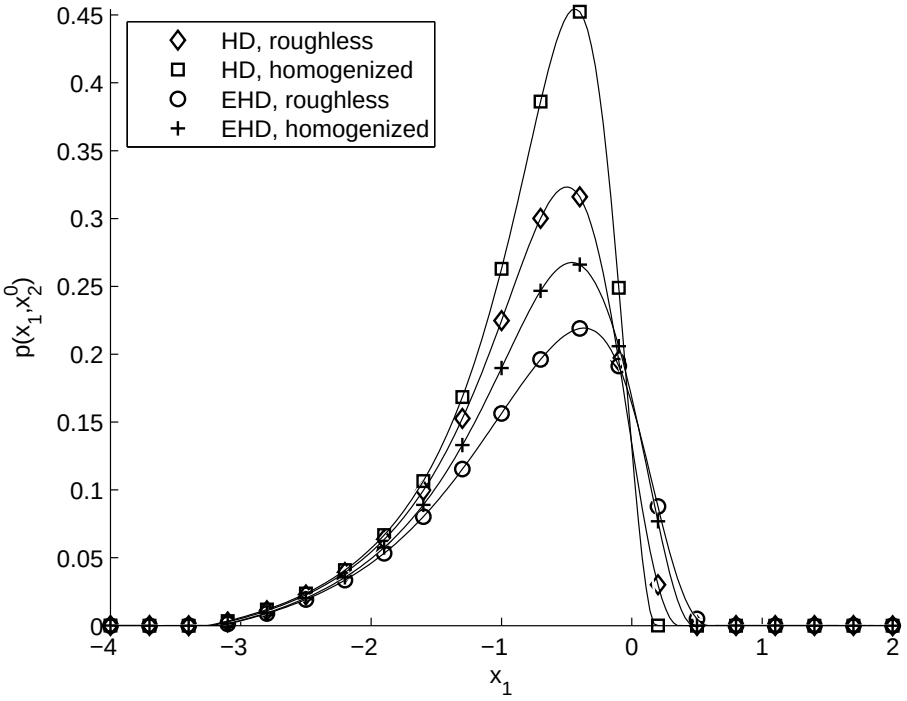

Fig. 18. Transverse roughness effects over the pressure in purely hydrodynamic and elastohydrodynamic cases at $x_2^0 = 0$

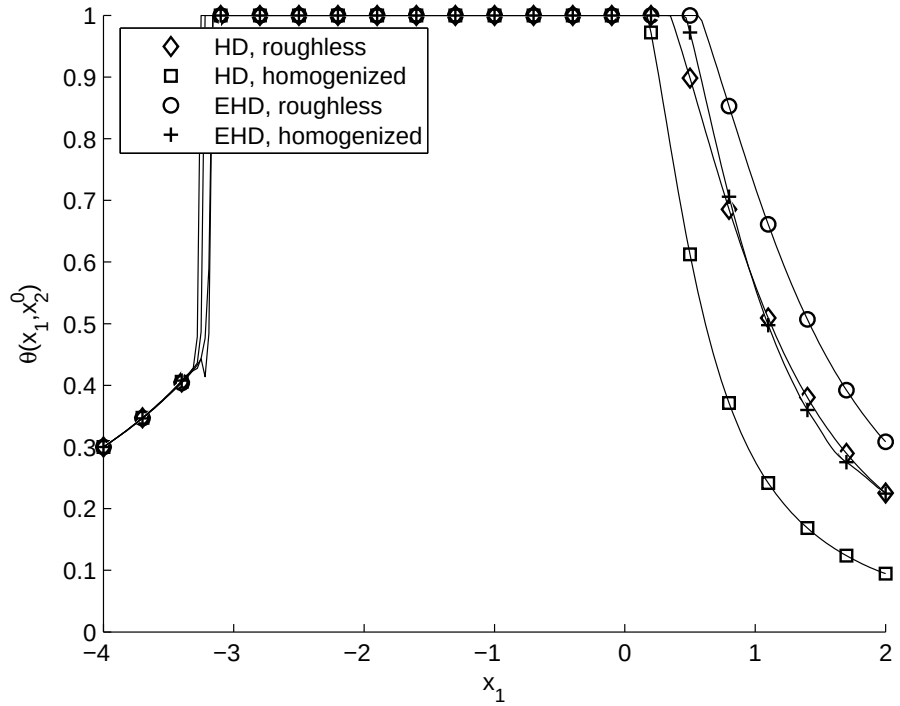

Fig. 19. Transverse roughness effects over the saturation in purely hydrodynamic and elastohydrodynamic cases at $x_2^0 = 0$

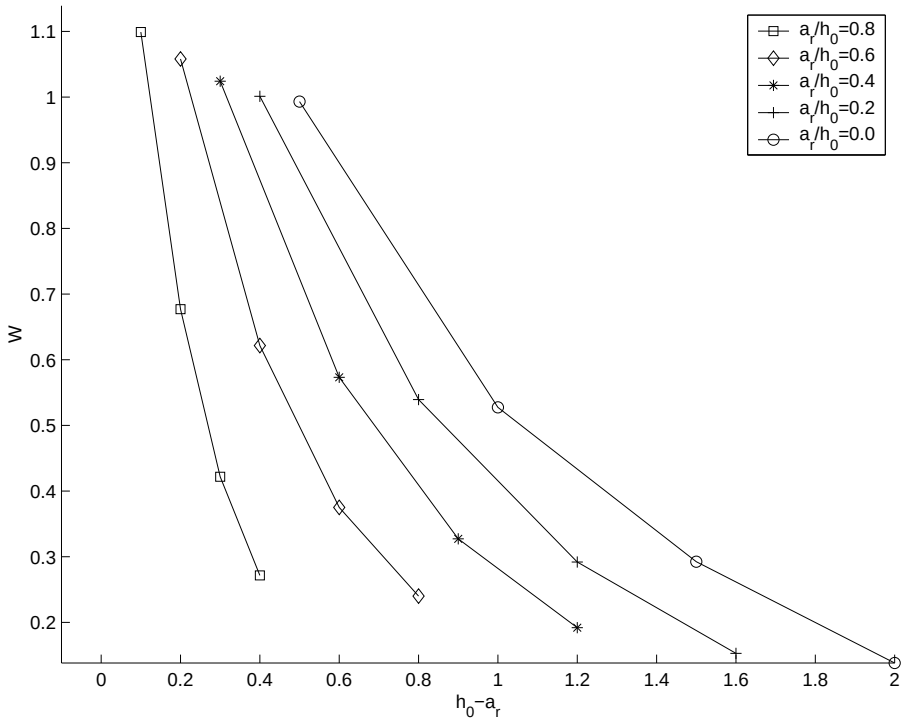

Fig. 20. Influence of the roughness over the load

a few variations affect the saturation distribution (for this reason, the corresponding curves are omitted).
TABLE 2 (resp. TABLE 3) gives the variation of the peak pressure (resp. deformation) with respect to the isoviscous case ($\alpha = 0$) in different rough cases (including roughless and homogenized ones).
The relative variation of the peak pressure is denoted

$$\Delta p/p = \frac{\max(p^\alpha) - \max(p^0)}{\max(p^0)}$$

where p^α (resp. p^0) denotes the pressure distribution corresponding to the piezoviscous regime $\alpha \neq 0$ (resp. isoviscous regime $\alpha = 0$). Similarly, the relative variation of the peak deformation is denoted

$$\Delta d/d = \frac{\max(d_f^\alpha) - \max(d_f^0)}{\max(d_f^0)}$$

where d_f^α (resp. d_f^0) denotes the deformation distribution corresponding to the piezoviscous regime $\alpha \neq 0$ (resp. isoviscous regime $\alpha = 0$).

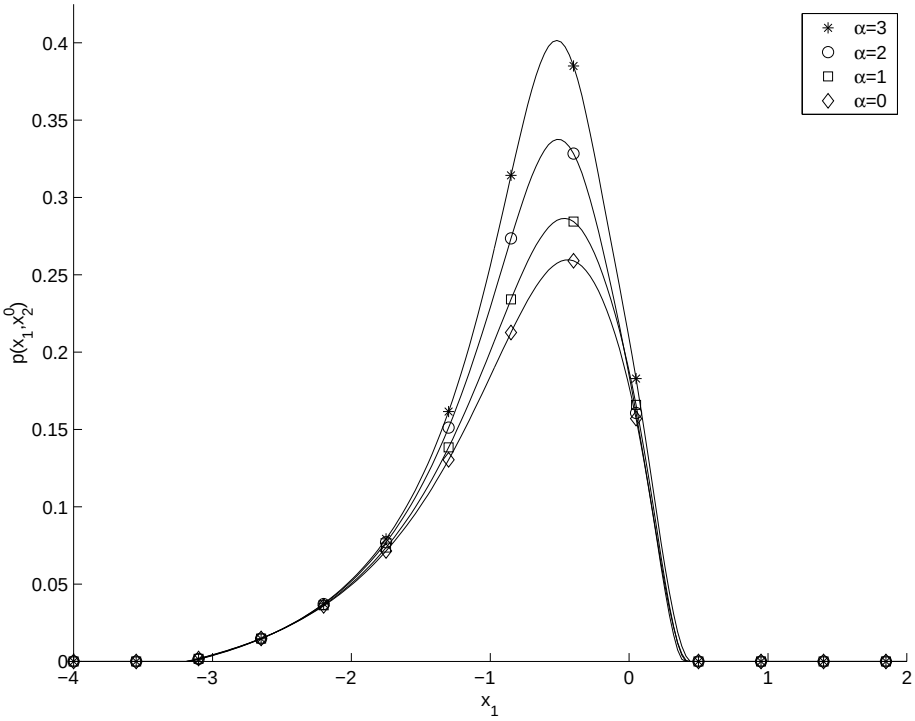

Fig. 21. Influence of the piezoviscosity over the (homogenized) pressure

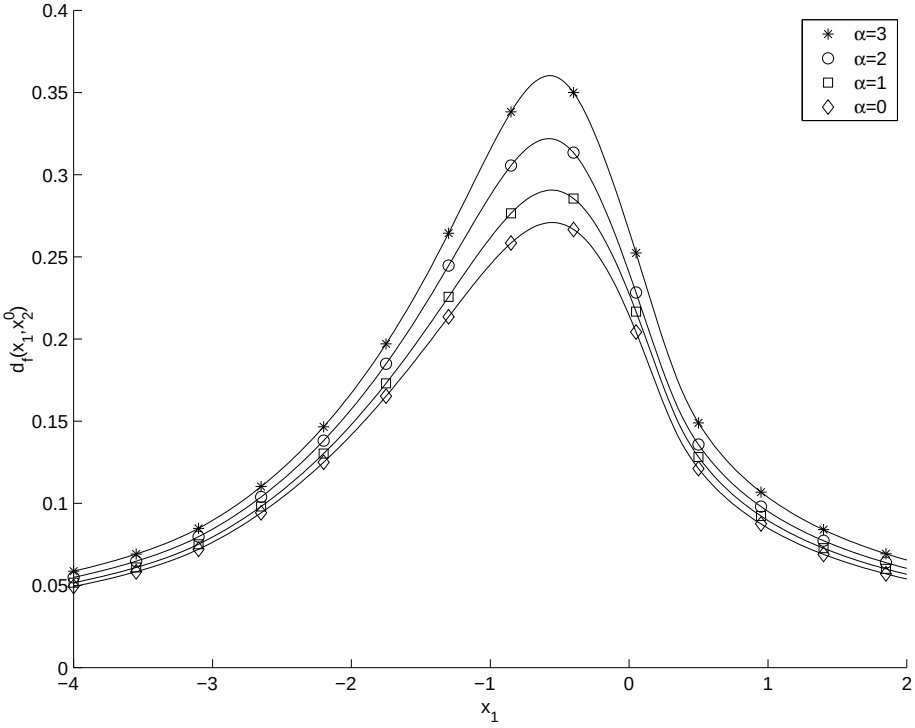

Fig. 22. Influence of the piezoviscosity over the (homogenized) deformation

$\Delta p/p$	$\alpha = 1$	$\alpha = 2$	$\alpha = 3$
roughless	0.0817	0.2633	0.4449
$\varepsilon = 1/10$	0.1035	1.8646	2.8203
$\varepsilon = 1/20$	0.2447	0.6551	1.0192
$\varepsilon = 1/30$	0.1855	0.5161	1.3783
homogenized	0.1041	0.3030	0.5543

Table 2
Maximum pressure elevation due to piezoviscosity

$\Delta d/d$	$\alpha = 1$	$\alpha = 2$	$\alpha = 3$
roughless	0.0540	0.1716	0.2787
$\varepsilon = 1/10$	0.0584	0.5742	0.6034
$\varepsilon = 1/20$	0.1078	0.2497	0.4532
$\varepsilon = 1/30$	0.0907	0.2198	0.4386
homogenized	0.0732	0.1895	0.3320

Table 3
Maximum deformation elevation due to piezoviscosity

5 Conclusion

The solution procedure for deterministic periodic roughness computation, which has been developped in [3], has been extended to the (piezoviscous) elastohydrodynamic case. It is valid for transverse or longitudinal roughness patterns. Further investigation has to be made in order to take into account anisotropic two dimensional effects.

References

[1] G. Bayada, J.-B. Faure, A double-scale analysis approach of the Reynolds roughness. Comments and application to the journal bearing, ASME J. of Tribology 111 (1989) 323–330.

[2] G. Bayada, S. Martin, C. Vázquez, Effets d'anisotropie par homogénéisation dans un problème à frontière libre, C. R. Math. Acad. Sci. Paris 340 (7) (2005) 541–546.

[3] G. Bayada, S. Martin, C. Vázquez, An average flow model of the Reynolds roughness including a mass-flow preserving cavitation model, ASME J. of Tribology (to appear).

[4] A. Kumar, J. F. Booker, A finite element cavitation algorithm, ASME J. of Tribology 113 (2) (1991) 276–86.

[5] F. Shi, R. F. Salant, A mixed soft elastohydrodynamic lubrication model with interasperity cavitation and surface shear deformation, ASME J. of Tribology 122 (2000) 308–316.

[6] D. Vijayaraghavan, T. G. Keith, An efficient, robust, and time accurate numerical scheme applied to a cavitation algorithm, ASME J. of Tribology 112 (1990) 44–51.

[7] D. Dowson, G. R. Higginson, Elastohydrodynamic lubrication, Pergamon Press, Oxford, Great Britain, 1977.

[8] G. Bayada, M. Chambat, C. Vázquez, Characteristics method for the formulation and computation of a free boundary cavitation problem, J. Comput. Appl. Math. 98 (2) (1998) 191–212.

[9] A. Bermúdez, J. Durany, La méthode des caractéristiques pour les problèmes de convection-diffusion stationnaires, RAIRO Modél. Math. Anal. Numér. 21 (1) (1987) 7–26.

[10] I. Arregui, J. J. Cendán, C. Vázquez, Mathematical analysis and numerical simulation of a Reynolds-Koiter model for the elastohydrodynamic journal-bearing device, M2AN Math. Model. Numer. Anal. 36 (2) (2002) 325–343.

[11] J. Durany, G. García, C. Vázquez, Numerical simulation of a lubricated Hertzian contact problem under imposed load, Finite Elem. Anal. Des. 38 (7) (2002) 645–658.